

Boundary scattering in the ϕ^6 model

Fred C. Lima¹, Fabiano C. Simas², K. Z. Nobrega³, Adalto R. Gomes^{1*}

¹ *Departamento de Física, Universidade Federal do Maranhão (UFMA)
Campus Universitário do Bacanga, 65085-580, São Luís, Maranhão,
Brazil* ² *Centro de Ciências Agrárias e Ambientais-CCAA,
Universidade Federal do Maranhão (UFMA),
65500-000, Chapadinha, Maranhão, Brazil*

³ *Departamento de Eletro-Eletrônica, Instituto Federal de Educação,
Ciência e Tecnologia do Maranhão (IFMA),
Campus Monte Castelo, 65030-005, São Luís, Maranhão, Brazil*

Abstract

We study the non-integrable ϕ^6 model on the half-line. The model has two topological sectors. We chose solutions from just one topological sector to fix the initial conditions. The scalar field satisfies a Neumann boundary condition $\phi_x(0, t) = H$. We study the scattering of a kink (antikinks) with all possible regular and stable boundaries. When $H = 0$ the results are the same observed for scattering for the same model in the full line. With the increasing of H , sensible modifications appear in the dynamics with of the defect with several possibilities for the output depending on the initial velocity and the boundary. Our results are confronted with the topological structure and linear stability analysis of kink, antikink and boundary solutions.

PACS numbers: 11.10.Lm, 11.27.+d, 98.80.Cq

*Electronic address: fredfjcl@gmail.com, simasfc@gmail.com, bzuzal@yahoo.com.br, argomes.ufma@gmail.com

I. INTRODUCTION

Solitary waves/solitons have a large number of realizations in several areas of physics [1, 2]. Despite simpler, models in $(1, 1)$ dimensions also have applicability in physics at all scales, from dark and bright solitons in cigar-shaped Bose-Einstein condensate [3] to high energy physics [4]. The kink (antikink) is the simplest solution with solitary character.

The solitary waves in integrable systems are characterized by a very simple behavior in kink-antikink collisions, with at most a phase shift in the field. Only solutions with this characteristic are defined as solitons in the mathematical literature, but in this paper we make no such restriction. The investigation of kink/antikink scattering in nonintegrable systems have since a long time showed some surprising results such as bion and two-bounce solutions. Several classes of nonintegrable models have already been studied. One can cite the polynomials ϕ^4 [5–11], ϕ^6 [12, 13], ϕ^8 [14], polynomials with extensions [15] or with an external perturbation [16] and nonpolynomials [17–23]. Interesting scattering structures where observed with multikinks [24–27] and with models with two scalar fields [28–31]. Despite the existence of analytical results for some classes of potentials [32], the study of kink scattering is mostly numerical.

As a first example, the nonintegrable ϕ^4 model presents a rich structure, which depends crucially in their initial velocity v_i [10]. For large initial velocity, above a critical value v_c , the pair $K\bar{K}$ recedes from each other, i.e, the kinks always escape to infinity after one collision. On the other hand, for initial velocities bellow v_c , the structure of the collision is far more complex. In this region, the kink and antikink capture one another, forming the bion state. For $v_i \lesssim v_c$ there is the possibility of scattering after a two-bouncing process, where the pair is again able to escape to infinity after colliding twice [5, 6, 8–11]. Each two-bounce process can be identified as corresponding to a particular two-bounce window. Such windows in velocity are characterized by widths that are reduced with the grow of v_i and accumulate around $v_i = v_c$. Near to each two-bounce windows usually there is a sequence of three-bounce windows. This structure is reproduced in a fractal pattern [10].

According to Campbell, Schonfeld and Wingate (CSW) [8], a collision presenting two-bounce is described by a resonance effect between the zero mode and the vibrational mode of the kink. Firstly there is the transferring of energy from the translational mode to the internal (vibrational) one. In the sequel, the energy is transferred back to the zero mode

and the kink-antikink pair is separated from their mutual attraction.

A counterexample of the CSW mechanism was found in Ref. [12] for the ϕ^6 model. There it was shown that certain antikink-kink collisions exhibit resonant scattering, even in the absence of a vibrational mode for one kink. This surprising result was related to the existence of a bound state produced by the antikink-kink pair [12]. A second counterexample was presented in Ref. [22], where some of us showed the total suppression of two-bounce windows, even with the presence of more than one vibrational mode.

The study of nonlinear field theories with boundary have a long tradition in integrable systems, mostly connected to the sine-Gordon model [33–38]. One object of investigation is to find suitable boundary conditions compatible with integrability [39]. Supersymmetric theories on the half-line keeping integrability were also considered [40–43]. One interesting aspect that deserves to be more investigated is the consequence of nonintegrability in the interaction of a kink or antikink with a boundary. In this line there are few examples of previous investigation for the ϕ^4 [44] and sine-Gordon [45] models.

The kink can be applied in scenarios with large symmetry in high energy physics. For instance, the collision of relativistic bubbles can be treated as planar walls and described as kink scattering in $(1, 1)$ dimensions [46–48]. Motivated by the undetection of topological defects expected to be produced at a large rate via the Kibble mechanism [49] in the early universe, the authors of the Ref. [50] investigated the ϕ^6 model under a generic perturbation. They showed that, due to the counterintuitive negative pressure effect, any small perturbation could trigger a chain reaction to influence the stability of a system of kinks. In this way the negative pressure can be the cause of the vanishing of domain walls in some models.

In condensed matter, the kink in a nonintegrable model was proposed theoretically in buckled graphene nanoribbon [51, 52]. The possibility of existence of the negative radiation pressure effect in buckled graphene was considered in the Ref. [53], based in the existence of such effect in a kink the ϕ^4 model [54]. The connection of solitons with conducting polymers is an active area of research, and some interesting reviews can be found Refs. [55, 56] (for a more gentle introduction to the subject, see the Ref. [57]). Kinks have an important role for describing the intriguing metallic properties of heavily doped *trans*-polyacetylene. In the Su-Schrieffer-Heeger (SSH) model [58], the kink/antikink excitations separate regions of two different classes of dimerization and satisfy the integrable sine-Gordon equation. These

defects are spinless and are formed upon charge transfer from the dopant to the polymer. The transition to a metallic state was explained by Kivelson and Heeger [59] as a crossover from a soliton lattice to a polaron lattice. Recently the interaction between the kink-antikink pair in photoexcited *trans*- polyacetylene was studied using ab-initio excited state dynamics [60]. After excited, the atoms evolve using an hybrid time-dependent density functional theory (TD-DFT). For $T = 0$ a soliton/antisoliton nucleates and pass through each other, as expected by a sine-Gordon model. For $T \neq 0$ a surprising result appears, with the solitons scattering after bouncing twice, a characteristic of a nonintegrable model. In an ideal conjugated polymer, a soliton is free to move because the total energy is independent on the position of the soliton. For finite chains, however, end effects push the soliton to the center of the chain. In the SSH theory, and for enlarged dimerization parameters, a linear term is introduced in the potential leading to these repulsive effects of the border [61, 62]. An extension of the SSH model to include a third-neighbor interaction [63] shows that all conformal excitations in both *cis*- and *trans*-polyacetylene are repelled from the chain ends.

In this paper, we will discuss the process of collision of antikinks and kinks in the ϕ^6 model with a Neumann boundary condition. Since the antikink (kink) ϕ^6 has no associated vibrational state, our main motivation was to investigate if the boundary condition is able to produce bounce windows. Our numerical analysis shows that this is the case for antikink-boundary scattering, with a very intricate structure emerging from the scattering process. The kink-boundary scattering leads to different results depending on the type of boundary to be scattered, with the most notable aspect the possibility of he changing of the topological sector and the nature of the boundary due to the scattering. Another motivation was to investigate if the boundary has a repulsive character to the scattering defect. We found that this is true in most cases, but for some configurations the defect can be “trapped” around or even annihilated by the boundary.

In the next section we review the first-order formalism for obtaining static solutions and stability analysis. The Sect. III reviews some known results of solutions and stability analysis for the ϕ^6 model in the full line. In the Sect. IV we present solutions and stability analysis in the half line. The numerical analysis of antikink boundary scattering is presented in the Sect. V. Corresponding results for kink boundary scattering is presented in the Sect. VI. We conclude in the Sect. VII.

II. BPS STATES

We consider the following action with standard dynamics

$$S = \int dxdt \left(\frac{1}{2} \partial_\mu \phi \partial^\mu \phi - V(\phi) \right). \quad (1)$$

The equation of motion is given by

$$\frac{\partial^2 \phi}{\partial t^2} - \frac{\partial^2 \phi}{\partial x^2} + V_\phi = 0, \quad (2)$$

where $V_\phi = dV/d\phi$. If the potential is

$$V(\phi) = \frac{1}{2} W_\phi^2, \quad (3)$$

the solutions of the first-order equation

$$\frac{d\phi}{dx} = \pm W_\phi, \quad (4)$$

are also static solutions of the second-order equation of motion. The defects formed with this prescription minimize energy, connect adjacent minima of the potential and are known as BPS defects [64, 65]. Stability analysis around a static solution $\phi_S(x)$ considers $\phi(x, t) = \phi_S(x) + \eta(x)e^{i\omega t}$ and the first-order corrections in the equation of motion. This results in a Schrödinger-like eigenvalue equation

$$-\frac{d^2 \eta(x)}{dx^2} + U(x)\eta(x) = \omega^2 \eta(x), \quad (5)$$

where the potential is

$$U(x) = \left. \frac{d^2 V(\phi)}{d\phi^2} \right|_{\phi=\phi_S}. \quad (6)$$

The Schrödinger-like equation can be rewritten as $\mathcal{H}\eta(x) = \omega^2 \eta(x)$. That is, linear stability is assured if the Hamiltonian \mathcal{H} is positive definite.

Now we consider the model on the half-line $-\infty < x < 0$. For this we consider the action

$$S = \int_{-\infty}^0 dx \int dt \left\{ \frac{1}{2} \partial_\mu \phi \partial^\mu \phi - V(\phi) + \delta(x) H \phi \right\}. \quad (7)$$

Varying the action with respect to ϕ leads to an equation of motion for $x \neq 0$ identical to Eq.(2) obtained previously for the full-line. In addition, when extended and considered around $x = 0$, the action gives the integrable Neumann condition

$$\left. \frac{d\phi}{dx} \right|_{x=0} = H. \quad (8)$$

Static solutions have energies given by

$$E = \int_{-\infty}^0 \left[\frac{1}{2} \left(\frac{d\phi}{dx} \right)^2 + V(\phi) \right] dx - H \phi(x=0), \quad (9)$$

or, by Eqs. (3) and (4),

$$E[\phi] = \pm W \Big|_{\phi(-\infty)}^{\phi(0)} - H \phi(0, t). \quad (10)$$

III. THE ϕ^6 MODEL ON THE FULL LINE

We consider the model given by

$$V(\phi) = \frac{1}{2} \phi^2 (1 - \phi^2)^2. \quad (11)$$

The associated superpotential is $W(\phi) = \phi^2/2 - \phi^4/4$. The first-order equations are then

$$\frac{d\phi}{dx} = \phi - \phi^3, \quad (12)$$

$$\frac{d\phi}{dx} = -(\phi - \phi^3). \quad (13)$$

Note that the potential has vacua given by $\{-1, 0, 1\}$. The kink connecting the minima $\{0, 1\}$ is given by [12]

$$\Phi_{1+}(x) = \sqrt{\frac{1 + \tanh(x)}{2}}. \quad (14)$$

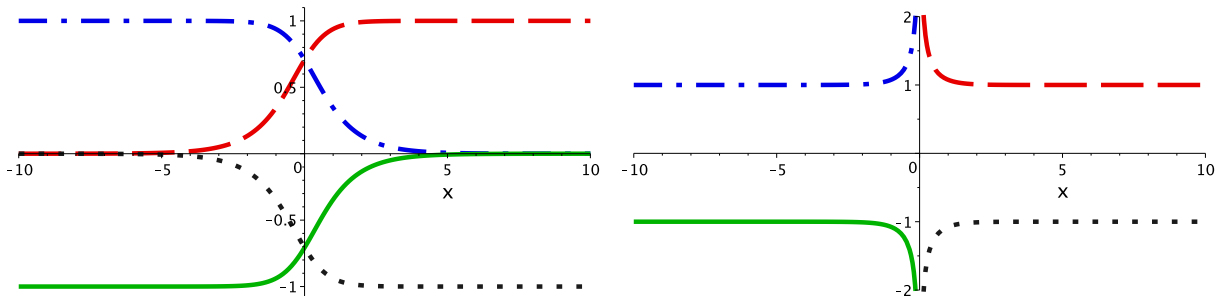


FIG. 1: The ϕ^6 model on the full line: a) (left) Static BPS kinks and antikinks on the full line, centered at $x = 0$. Plots are for $\Phi_{1+}(x)$ (red dashed), $\Phi_{2+}(x)$ (blue dash dotted), $\Phi_{1-}(x)$ (black dotted), $\Phi_{2-}(x)$ (green solid line). b) (right) Irregular solutions $\Phi_{3+}(x)$ (red dashed), $\Phi_{4+}(x)$ (blue dash dotted), $\Phi_{3-}(x)$ (black dotted), $\Phi_{4-}(x)$ (green solid line).

The antikink connecting the minima $\{1, 0\}$ is given by [12]

$$\Phi_{2+}(x) = \sqrt{\frac{1 - \tanh(x)}{2}}. \quad (15)$$

The antikink and kink connecting the minima $\{0, -1\}$ and $\{-1, 0\}$ are given, respectively, by $\Phi_{1-}(x) = -\Phi_{1+}(x)$ and $\Phi_{2-}(x) = -\Phi_{2+}(x)$. Each of these solutions has energy $E = 1/4$, and their profiles can be seen in Fig. 1a. In addition we have four other solutions of the second-order equation of motion, divergent at $x = 0$:

$$\Phi_{3\pm}(x) = \pm \sqrt{\frac{1 + \coth(x)}{2}} \quad (16)$$

$$\Phi_{4\pm}(x) = \pm \sqrt{\frac{1 - \coth(x)}{2}}. \quad (17)$$

The profile of these solutions are presented in Fig. 1b.

Stability analysis for $\Phi_{1\pm}$ leads to the following potential of perturbations:

$$U_1(x) = \frac{5}{2} + \frac{3}{2} \tanh(x) - \frac{15}{4} \text{sech}^2(x). \quad (18)$$

Similarly, for $\Phi_{2\pm}$ we have

$$U_2(x) = \frac{5}{2} - \frac{3}{2} \tanh(x) - \frac{15}{4} \text{sech}^2(x). \quad (19)$$

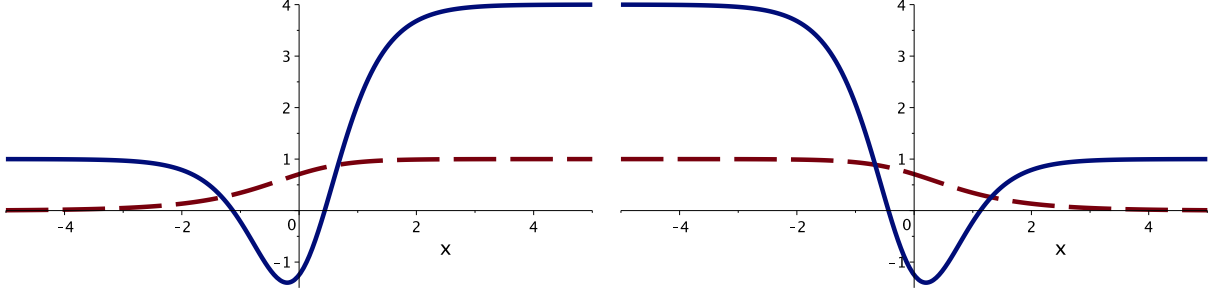


FIG. 2: The ϕ^6 model on the full line: Schrödinger-like potential (solid line) and scalar field profile (traced line) for a) (left) kink Φ_{1+} and b) (right) antikink Φ_{2+} . See Ref. [12]

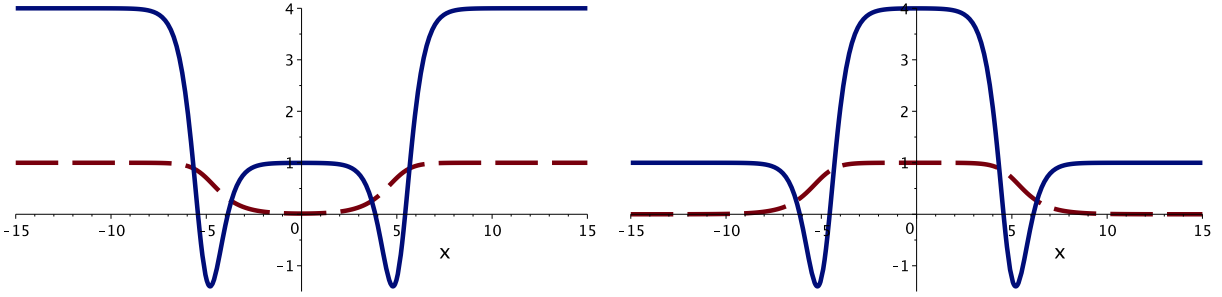


FIG. 3: The ϕ^6 model on the full line: Schrödinger-like potential (solid line) and scalar field profile (traced line) for a) (left) antikink-kink (composite system $\Phi_{1+}(x-a) + \Phi_{2+}(x+a)$) and b) (right) kink-antikink (composite system $\Phi_{1+}(x-a) + \Phi_{2+}(x+a) - 1$). Here we considered $a = 5$.

Figs. 2 a-b show the plots of the potentials. There one can see three characteristic regions: i) $0 < \omega^2 < 1$ where one can look for bound states, ii) $1 < \omega^2 < 4$ where there is a continuum of reflecting states and iii) $\omega^2 > 4$ where there is a continuum of free states. In particular, the analysis of these states for $\Phi_{1\pm}$ was presented in detail in the Ref. [66] (see also Ref. [67]). The potentials have just one bound state, the zero-mode connected with the translational symmetry of the solutions. According to the CSW mechanism [8], the absence of a vibrational state would result in the absence of two-bounce windows in collisions involving kinks (or antikinks). However, an interesting counterexample was presented in Ref. [12]. In their paper the authors showed the presence of bounce windows in antikink-kink collisions. The explanation was that the energy after the initial impact was trapped in the composited antikink-kink configuration. For example, the composite antikink-kink system given by $\phi(x) = \Phi_{2+}(x+a) + \Phi_{1+}(x-a)$ has a potential of perturbations represented in Fig. 3a. This potential has a tower of bound states. On the contrary, the kink-antikink system given by $\phi(x) = \Phi_{1+}(x+a) + \Phi_{2+}(x-a) - 1$ has the Schrödinger-like potential showed in

Fig. 3b. There one has only two quasi-zero modes. That is the reason why bounce windows are absent in kink-antikink collisions.

IV. THE ϕ^6 MODEL ON THE HALF-LINE

Now we consider the ϕ^6 model on the half-line $-\infty < x < 0$. Firstly we will consider the solutions given by

$$\varphi_{1+}(x) = \sqrt{\frac{1 + \tanh[x - \chi(H)]}{2}}, \quad (20)$$

$$\varphi_{4+}(x) = \sqrt{\frac{1 - \coth[x - X_1(H)]}{2}}, \quad (21)$$

which correspond respectively to $\Phi_{1+}(x)$ and $\Phi_{4+}(x)$ on the full line. The Neumann condition (Eq. (8)), impose that

$$\frac{\operatorname{sech}^2 \chi}{\sqrt{8 - 8 \tanh \chi}} = H, \quad (22)$$

$$\frac{\coth X_1^2 - 1}{\sqrt{8 + 8 \coth X_1}} = H. \quad (23)$$

The Eqs. (22) and (23) have no real solutions for $H < 0$. The Eq. (22) has two solutions for each value of H in the interval $0 \leq H \leq H_m$, where $H_m = 2/\sqrt{27}$. We will call these solutions of $X_0(H)$ and $\hat{X}_0(H)$ with $\hat{X}_0 \leq X_0$. For $H = H_m$ we have $\hat{X}_0 = X_0$. As a comparison, for the ϕ^4 model on the half-line we have [44] $|\hat{X}_0| = |X_0|$ and $H_m = 1$. In addition the Eq. (23) has a unique real solution for $X_1(H)$ in the interval $0 < H < \infty$. Similar reasoning can be done with the solutions

$$\varphi_{2+}(x) = \sqrt{\frac{1 - \tanh[x + \chi(H)]}{2}}, \quad (24)$$

$$\varphi_{3+}(x) = \sqrt{\frac{1 + \coth[x + X_1(H)]}{2}}. \quad (25)$$

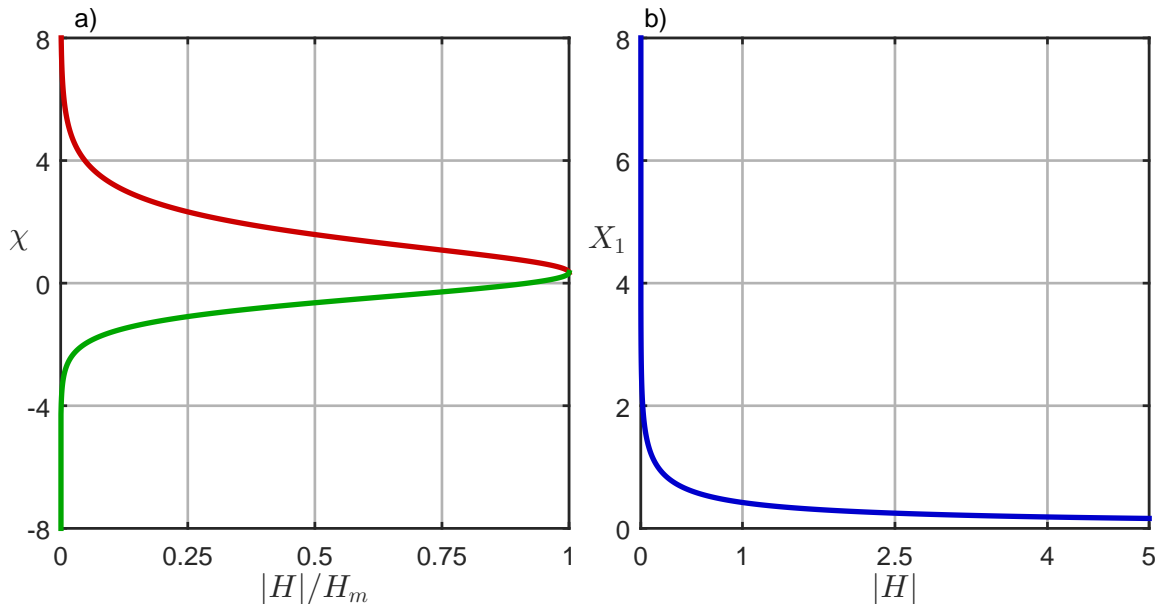


FIG. 4: a) The two real solutions of Eq. (26) for $\chi(H)$: X_0 (red) and \hat{X}_0 (green); b) the unique real solution $X_1(H)$ of Eq. (27).

In this case the Neumann condition (Eq. (8)) gives also Eqs. (22) and (23).

$$\frac{\operatorname{sech}^2 \chi}{\sqrt{8 - 8 \tanh \chi}} = -H, \quad (26)$$

$$\frac{\operatorname{coth} X_1^2 - 1}{\sqrt{8 + 8 \operatorname{coth} X_1}} = -H. \quad (27)$$

The Eqs. (26) and (27) have no real solutions for $H > 0$. The Eq. (26) has two solutions, $X_0(H)$ and $\hat{X}_0(H)$ in the interval $-H_m \leq H \leq 0$ whereas Eq. (27) has one solution for each value of $H < 0$. The Fig. 4a presents the behavior the parameters X_0 and \hat{X}_0 as function of $|H|/H_m$. The Fig. 4b presents the parameter X_1 as function of $|H|$. In the figures the signal of H depends on the particular φ_{i+} , $i = 1..4$.

We can classify the solutions depending on the BPS equations they satisfy. Then we have

$$\phi_1(x) = \sqrt{\frac{1 + \tanh(x - X_0)}{2}} \quad (28)$$

$$\phi_2(x) = \sqrt{\frac{1 + \tanh(x - \hat{X}_0)}{2}} \quad (29)$$

$$\phi_3(x) = \sqrt{\frac{1 + \operatorname{coth}(x + X_1)}{2}}. \quad (30)$$

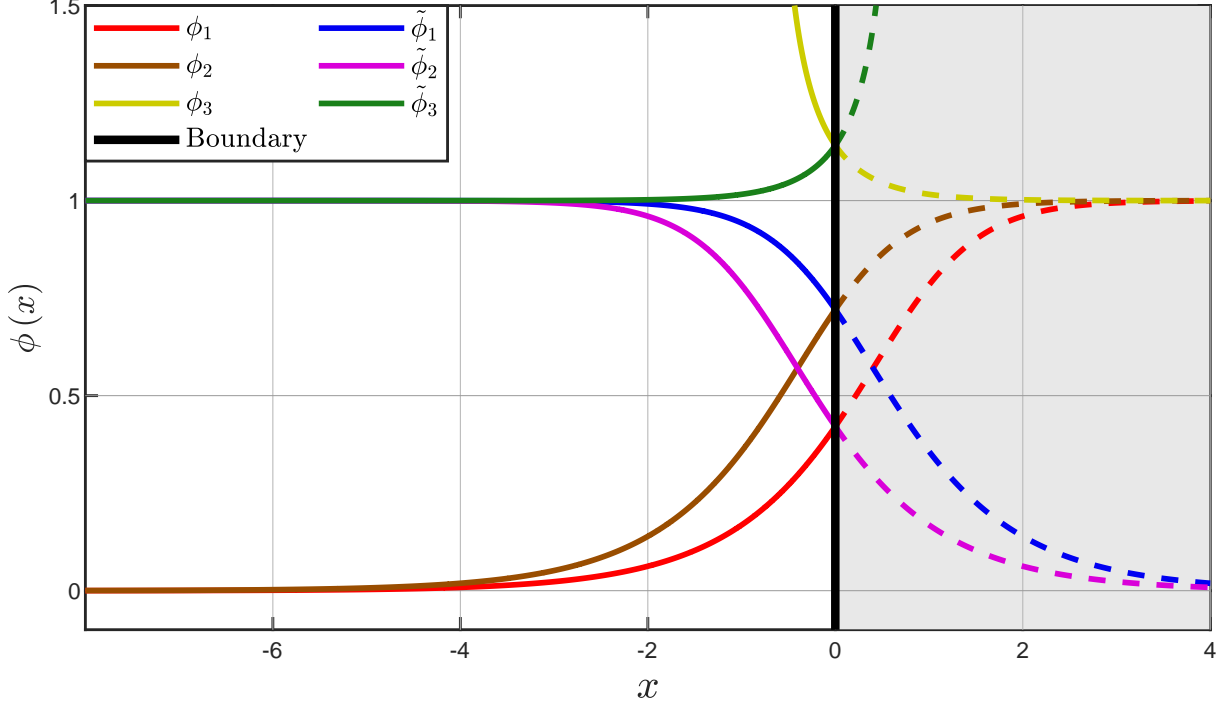


FIG. 5: Static solutions for $|H| = 0.90H_m$.

which satisfy BPS Eq. (12). Also we have

$$\tilde{\phi}_1(x) = \sqrt{\frac{1 - \tanh(x + \hat{X}_0)}{2}} \quad (31)$$

$$\tilde{\phi}_2(x) = \sqrt{\frac{1 - \tanh(x + X_0)}{2}}, \quad (32)$$

$$\tilde{\phi}_3(x) = \sqrt{\frac{1 - \coth(x - X_1)}{2}}, \quad (33)$$

which satisfy BPS Eq. (13). Note that ϕ_1, ϕ_2 and $\tilde{\phi}_3$ are solutions for $H > 0$ whereas $\tilde{\phi}_1, \tilde{\phi}_2$ and ϕ_3 are solutions for $H < 0$.

The profiles of the solutions in the region $x < 0$ are depicted in the Fig. 5. Solution $\phi_3(x)$ is not regular for $x < 0$ and will not be considered here. The energy of static solutions can be found using Eq. (10). Then, the energies for solutions (28 - 29) are given by

$$E[\phi_i(x)] = \frac{3}{4}\phi_i(0)^4 - \frac{1}{2}\phi_i(0)^2, \quad (34)$$

with $i = 1 \dots 2$ whereas those for solutions (31 - 33) are given by

$$E[\tilde{\phi}_i(x)] = \frac{1}{4} + \frac{1}{2}\tilde{\phi}_i(0)^2 - \frac{3}{4}\tilde{\phi}_i(0)^4 \quad (35)$$

with $i = 1 \dots 3$. The Eqs. (34) and (35) shows that the energies presents an implicit dependence with H through of $\phi_i(0)$ and $\tilde{\phi}_i(0)$.

The Fig. 6 shows the Schrödinger-like potential for some static configurations of antikink-boundary and kink-boundary for several values of H . Note from the figure that potential is composed of two parts: one, with a hole centered at x_0 (chosen as -12.5 in the figure), characterizes the kink/antikink defect (known to have only the translational mode $\omega^2 = 0$); the second one, close to $x = 0$, represents the influence of the boundary. Note also that for $\omega^2 > 4$ one has a continuum of states. The possibility of vibrational states depends on the boundary. The Figs. 6a-b shows that, for the boundaries ϕ_1 and ϕ_2 , vibrational states must be searched for $\omega^2 \leq 4$. On the other hand, the potentials of the Figs. 6c-d show that true vibrational states can occur for $\omega^2 < 4$; for $1 < \omega^2 < 4$ we have metastable states, similar to the reflecting states in the full line of Sect. III.

In order to study the occurrence of localized boundary modes, we solve numerically the Schrödinger-like equation when the defect is too far from the boundary. The Fig. 7 shows the squared frequency of these modes as a function of H . For $0 < H < H_m$, we analyzed the solutions $\phi_1(x)$, $\phi_2(x)$ and $\tilde{\phi}_3(x)$. For $\phi_1(x)$ we have one vibrational state with $0 < \omega^2 < 1$ and the solution is stable. For $\phi_2(x)$ we have one mode with $\omega^2 < 0$, meaning instability. The solution $\tilde{\phi}_3(x)$ has no bound states, meaning also no signal of instability. For $-H_m < H < 0$ we analyzed the solutions $\tilde{\phi}_1(x)$ and $\tilde{\phi}_2(x)$. For $\tilde{\phi}_1(x)$ there is one state with $\omega^2 > 0$ and the solution is stable. The classification of this state depends on the value of H . The Fig. 7 shows that for $-0.90 \lesssim H/H_m < 0$ we have $1 < \omega^2 < 4$. When we consider the whole system antikink-boundary, this is in fact a metastable state, as already discussed. For $-1 < H/H_m \lesssim -0.90$ we have $0 < \omega^2 < 1$ and the solution is a true vibrational state of the boundary. The solution $\tilde{\phi}_2(x)$ has three bound states, one of them with $\omega^2 < 0$, meaning instability.

The stability of the boundaries was also analyzed numerically, considering only each boundary isolated, without any scattering process. Set $\xi(x)$ one of the boundaries

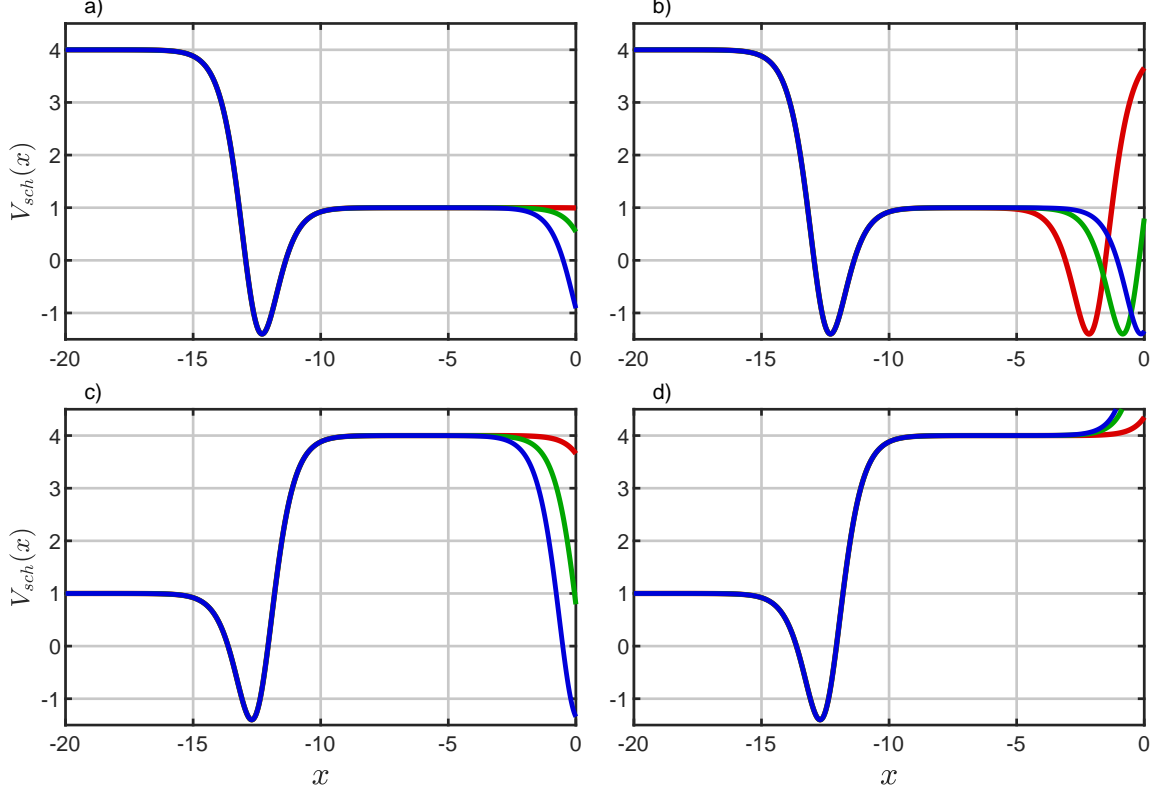


FIG. 6: Schrödinger-like potential for static configurations: a) $\Phi_{2+}(x - a) + \phi_1(x)$ b) $\Phi_{2+}(x - a) + \phi_2(x)$ c) $\Phi_{1+}(x - a) + \tilde{\phi}_1(x) - 1$ d) $\Phi_{1+}(x - a) + \tilde{\phi}_2(x) - 1$. The lines are for $|H| = 0.05H_m$ (red), $|H| = 0.50H_m$ (green) and $|H| = 0.95H_m$ (blue). We fix $a = -12.50$.

$\phi_1(x)$, $\tilde{\phi}_1(x)$, ϕ_2 and $\tilde{\phi}_3(x)$. The initial conditions are

$$\phi(x, 0) = \xi(x), \quad (36)$$

$$\dot{\phi}(x, 0) = 0. \quad (37)$$

For the numerical solutions we used a 4th-order finite-difference method on a grid $N = 2048$ nodes with the “infinity” at $x_{min} = -100$ and a spatial step $\delta x \approx 0.05$. For the time dependence we used a 6th order symplectic integrator method, with a time step $\delta t = 0.02$. We found no modification of the boundaries $\phi_1(x)$, $\tilde{\phi}_1(x)$ and $\tilde{\phi}_3(x)$ with the increasing of H even for large times, which is compatible with stability (see the Figs. 8a-b for the boundaries $\phi_1(x)$ and $\tilde{\phi}_3(x)$). On the other hand the instability of the $\phi_2(x)$ shows up in the simulations. One sees, for $H \lesssim 0.72$, the emission of radiation by the boundary, as shown for instance in the Fig. 8c. For $H \gtrsim 0.72H_m$ one has the production of a kink by the boundary, as shown

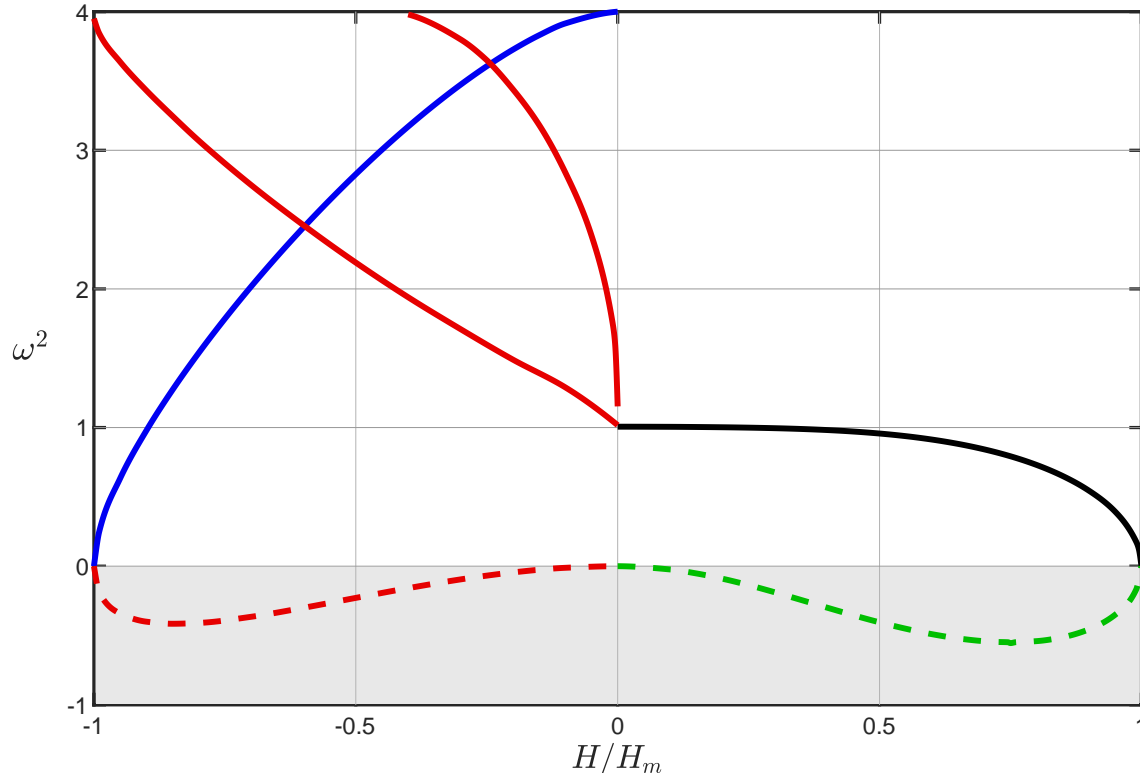


FIG. 7: The squared frequencies ω^2 of localised boundary modes as a function of H . The curves are for solutions $\phi_1(x)$ (black solid line) and $\phi_2(x)$ (green dashed line), $\tilde{\phi}_1(x)$ (blue solid line) and $\tilde{\phi}_2(x)$ (red dashed and solid lines).

for instance in the Fig. 8d. For such high values of H there is no emission of radiation before or after the production of the kink. In this case the effect of instability shows up abruptly, with no signal of instability thereafter. This is compatible with a decaying of the unstable ϕ_2 boundary to the stable ϕ_1 .

In the remaining of this work we will study of boundary scattering in the ϕ^6 model. For this purpose only the regular and stable solutions $\phi_1(x)$, $\tilde{\phi}_1(x)$ and $\tilde{\phi}_3(x)$ will be considered. We will see that even these stable boundaries can emit radiation, produce a kink/antikink or even change their nature due to the scattering. Clearly this is a consequence of the interaction defect-boundary, not a signal of instability.

V. ANTIKINK-BOUNDARY SCATTERING

Here we will consider scattering with an antikink in the sector $(0, 1)$ with the boundary. The Fig. 5 shows that an antikink in this sector can be connected with solutions $\phi_1(x)$ and

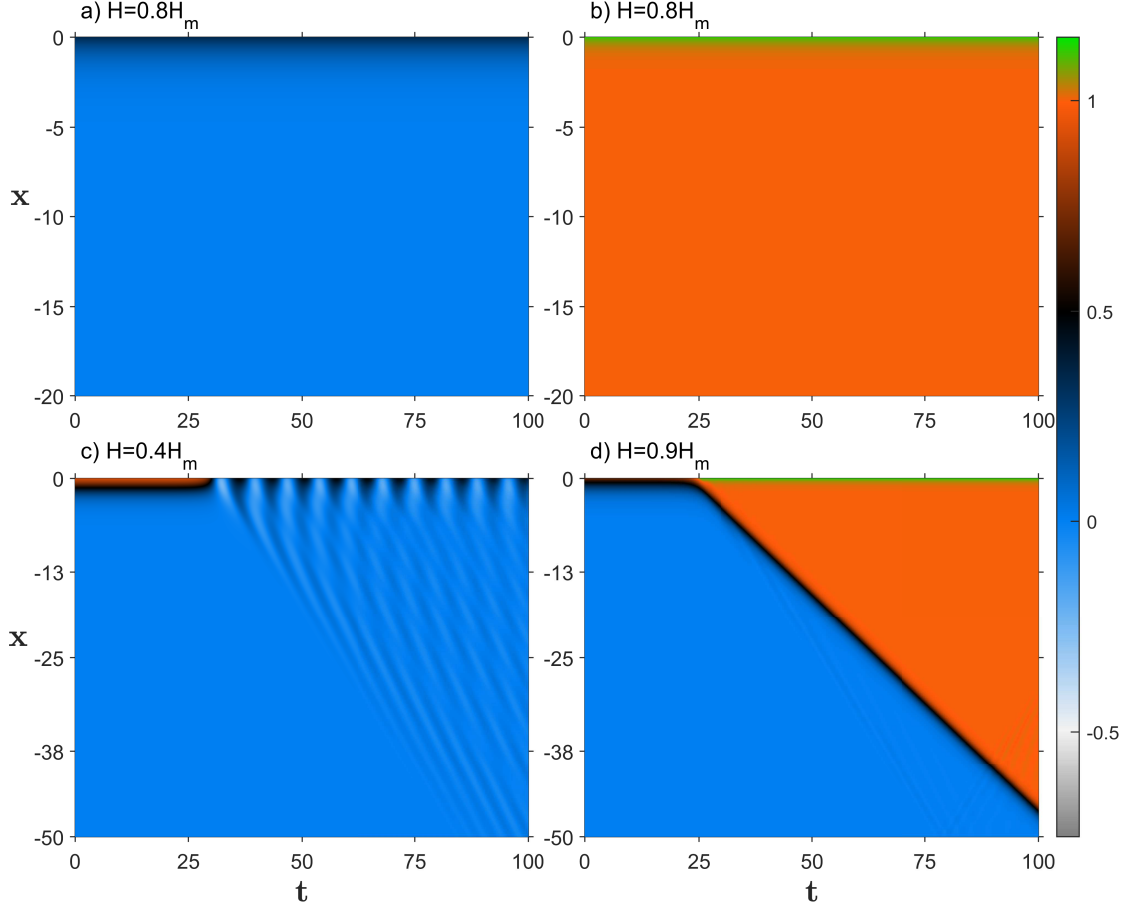


FIG. 8: Stability analysis of the boundaries: a) unchanging of $\phi_1(x)$ configuration, compatible with stability; b) unchanging of $\tilde{\phi}_3(x)$ configuration, compatible with stability; c) emission of radiation by the unstable ϕ_2 boundary; d) emission of a kink by the unstable ϕ_2 boundary. The values of H are shown in the figures.

$\phi_2(x)$, but only $\phi_1(x)$ is regular and stable. This means to restrict the parameter H to the range $0 < H < H_m$. The antikink is the static solution $\Phi_{2+}(x)$ given by the Eq. (15), now boosted with a velocity v_i with $x(t=0) = a$ and given by:

$$\Phi_{2+}(v_i, x, t) = \sqrt{\frac{1 - \tanh(\gamma(x - v_i t - a))}{2}} \quad (38)$$

with $\gamma = 1/\sqrt{1 - v_i^2}$. The initial conditions are

$$\phi(x, 0) = \Phi_{2+}(v_i, x, 0) + \phi_1(x), \quad (39)$$

$$\dot{\phi}(x, 0) = \dot{\Phi}_{2+}(v_i, x, t)|_{t=0}. \quad (40)$$

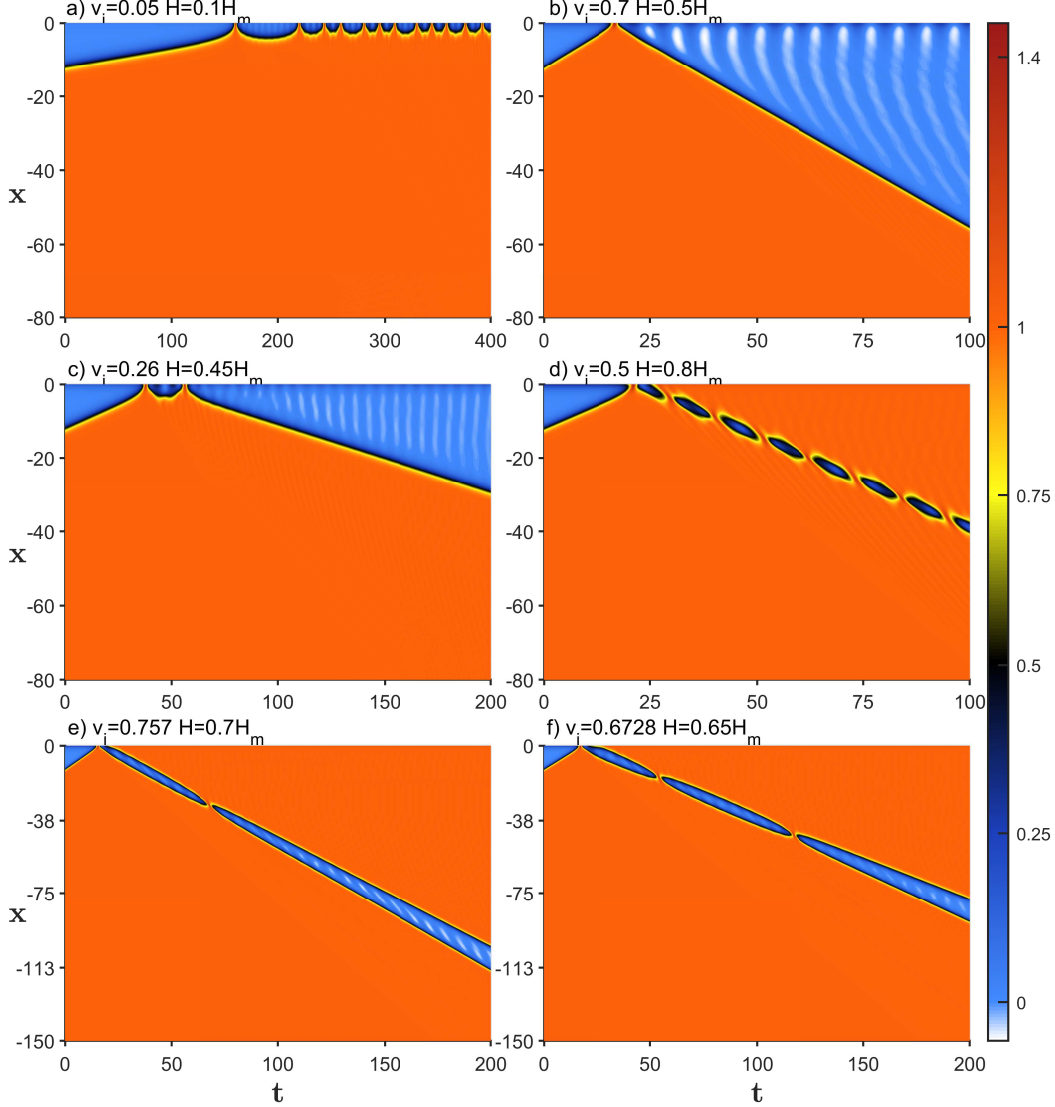


FIG. 9: $\Phi_{2+}(x)$ antikink scattering with ϕ_1 boundary, showing a) bion state at the boundary, b) inelastic scattering (one-bounce) with the boundary, c) two-bounce collision with the boundary, d) production of a $\Phi_{1+}(x)$ kink from the boundary, forming a composed oscillating state, e) production of a $\Phi_{1+}(x)$ kink from the boundary, showing the antikink colliding once with the formed kink, f) production of a $\Phi_{1+}(x)$ kink from the boundary, showing the antikink colliding twice with the formed kink. One can localize the structure of the output field profile at the boundary in the next Fig. 10.

For the numerical solutions we used $a = -12.5$ and a 4th-order finite-difference method. For the time dependence we used a 6th order symplectic integrator method.

The Fig. 9 shows the richness of possibilities of the scattering products. The realization of each scenario depends on the parameters (v_i, H) . The Fig. 9a shows a bion state at the boundary. Fig. 9b shows an inelastic scattering (one-bounce) with the boundary. Fig.

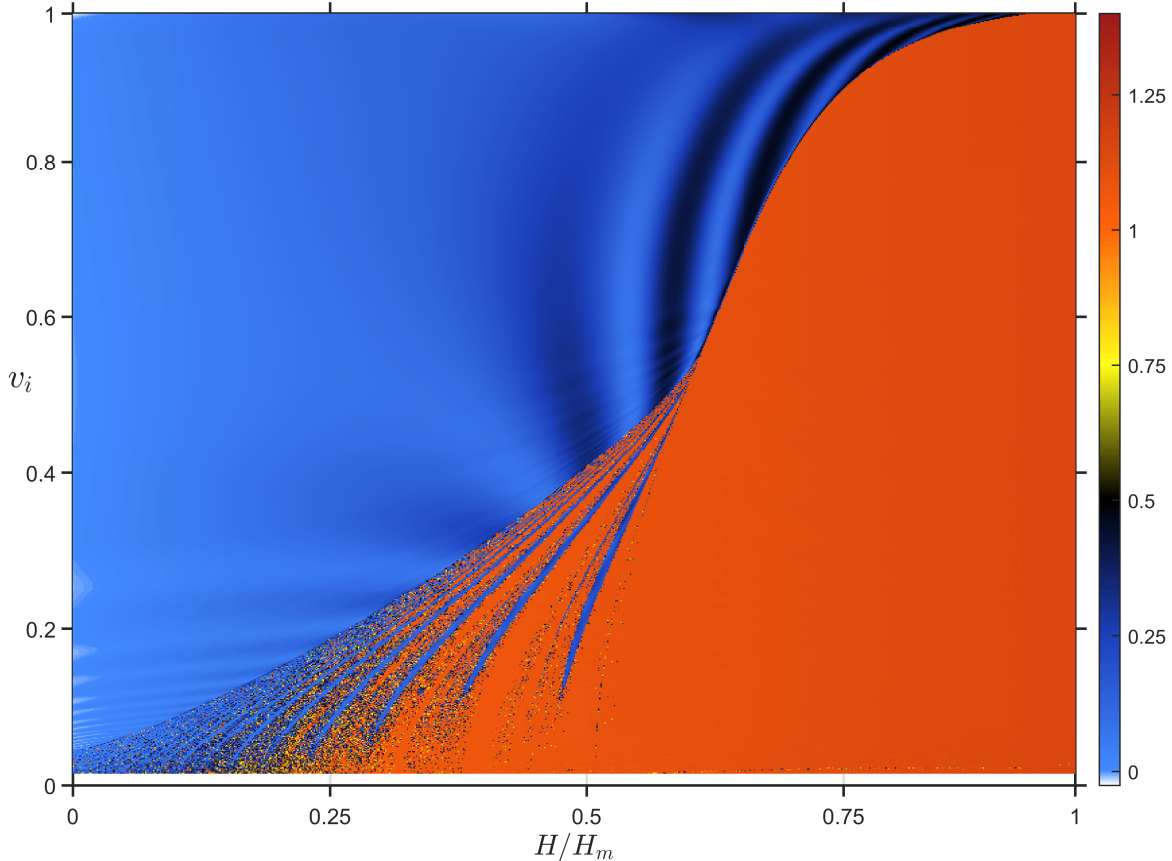


FIG. 10: $\Phi_{2+}(x)$ antikink scattering with ϕ_1 boundary: final state of the scalar field $\phi(0, t_f)$, with $t_f = |a|/v_i + 100$.

9c shows a two-bounce collision with the boundary. The Fig. 9d shows the production of a $\Phi_{1+}(x)$ kink by the boundary together with an inelastic scattering of the antikink. Note that the antikink-kink pair do not separate completely, forming a composed oscillating state. The Figs. 9e (9f) show cases where the produced $\Phi_{1+}(x)$ kink scatter once (twice) with the reflected antikink. After this collision, the separation between antikink and kink grows slowly with time, favoring the exchanging of radiation between the antikink-kink pair.

The contribution of the bound states to bion and two-bounce windows can be seen in the Figs. 9a and 9c. There we can see that between bounces there is emission of radiation whose frequency decreases with H . This agrees with the Fig. 7 (black curve). The same effect is observed in the pattern of the oscillations at the boundary after the scattering (compare the Figs. 9c and 9b).

The structure of our results on the boundary is presented in the Fig. 10. There one can see, in the bidimensional (H, v_i) phase space, the final state of the scalar field at $x = 0$.

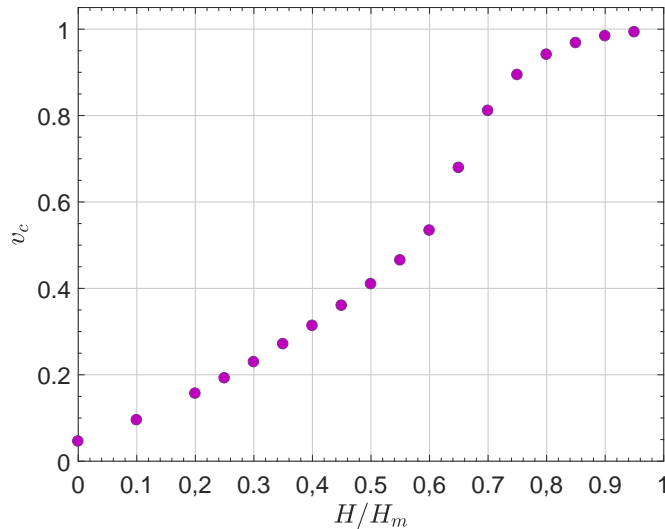


FIG. 11: $\Phi_{2+}(x)$ antikink scattering with ϕ_1 boundary: critical velocity v_c as a function of H . For $v_i > v_c$ there is no possibility of formation of a travelling kink at the boundary (see also Fig. 10).

In the blue region the antikink is inelastically scattered by the boundary after one bounce. The red region characterizes the production of a $\Phi_{1+}(x)$ kink by the boundary. In the figure we can observe the dependence with H of the structure of bounce windows. There the bounce windows are characterized by the finite intervals in blue ($\phi(0, t_f) \sim 0$) in the region $0 < H \lesssim 0.6H_m$, $v_i \lesssim 0.55$. The frontier red-blue characterizes the critical velocity v_c , above which the antikink collides only once with the boundary, thereafter retreating to $x \rightarrow -\infty$ (one can better visualize this in the Fig. 11). This is the analogous situation of a one-bounce solution for antikink-kink scattering in the full line. For velocities $v_i < v_c$ there are several possibilities: i) bion states with bounce windows for $v_i \lesssim v_c$. This is mostly observed for small values of H (left side of Fig. 10). ii) production of kink by the boundary for large values of H (right side of Fig. 10).

Fig. 11 shows the behavior of the critical velocity as a function of the parameter H . Note that the larger is H , the larger is the critical velocity. In particular, in the limit $H \rightarrow H_m$ we have $v_c \rightarrow 1$ and the formation of a travelling kink at the boundary. Note also that the curve v_c versus H presents an inflection point around $H \simeq 0.6H_m$, which coincides with the maximum value where two bounce windows are observed. For $H \gtrsim 0.6H_m$, v_c grows with H at a higher rate, favoring the occurrence of kink emission by the boundary.

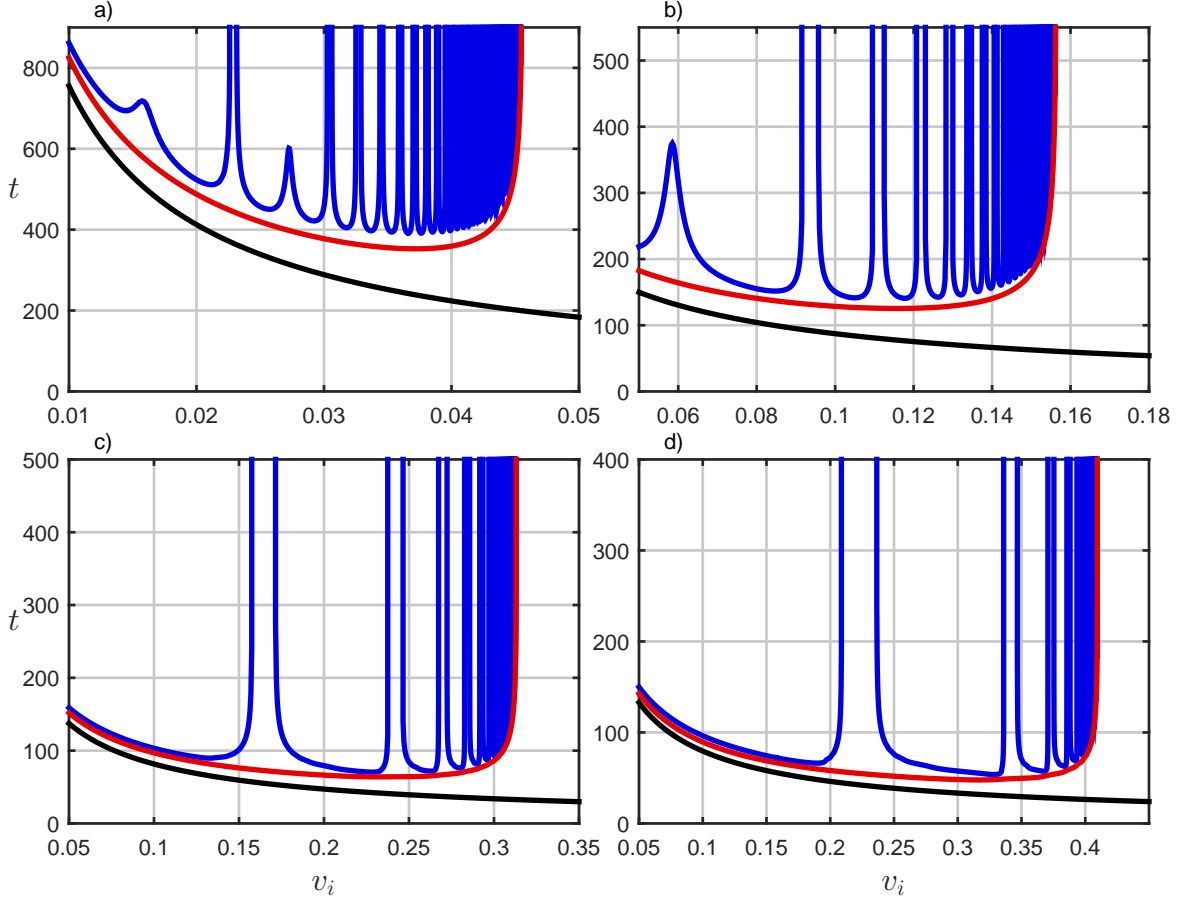


FIG. 12: $\Phi_{2+}(x)$ antikink scattering with ϕ_1 boundary: time of the first (black), second (red) and third (blue) bounce *versus* initial velocity for (a) $H = 0$, (b) $H = 0.2H_m$, (c) $H = 0.4H_m$, and (d) $H = 0.5H_m$.

The effect of H on the structure of two-bounce windows is described in the Figs. 12a-12d, where we see the times for the first three bounces as a function of the initial velocity. The two-bounce windows are delimited by divergences in the curves of the time of the third bounce. First of all, we observe that when $H = 0$ we recover the structure of two-bounce windows presented in antikink-kink scattering for the ϕ^6 model in the full line, as described in the Ref. [12]. As H grows from zero, also grows the critical velocity v_c that separated one-bounce inelastic scattering from bion states. We note also that with the grow of H the two-bounce windows accumulate around $v_i = v_c$. For $H \simeq 0.6H_m$ they disappear, remaining just the phenomena of kink production on the boundary.

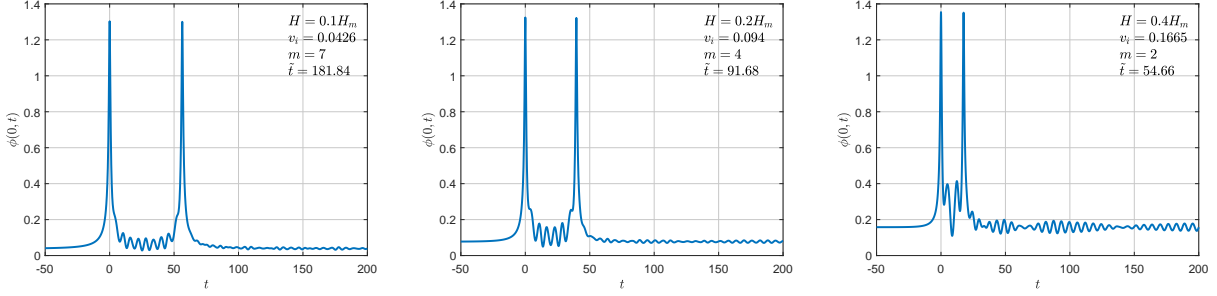


FIG. 13: $\Phi_{2+}(x)$ antikink scattering with ϕ_1 boundary: scalar field at the boundary $\phi(0, t)$ as a function of t for collisions from the first visible two-bounce window. a) $H = 0.1H_m$, b) $H = 0.2H_m$, c) $H = 0.4H_m$. The number m of oscillations between bounces for the first visible two-bounce windows is also indicated. In each figure the time t was rescaled as $t - \tilde{t}$ such that $t = 0$ corresponds to the first peak.

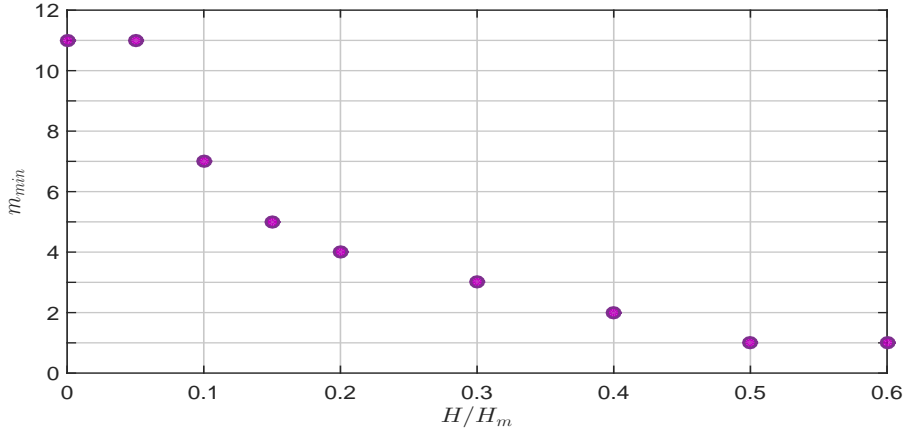


FIG. 14: $\Phi_{2+}(x)$ antikink scattering with ϕ_1 boundary: order of first two-bounce windows as a function of H/H_m .

One remarkable effect of the variation of H is indicated by the integer m , the number of oscillations between bounces of $\phi(0, t)$ for the first visible two-bounce windows. This can be seen in the Figs. 13 and 14. For small values of H ($H \leq 0.1H_m$), the structure of bounce windows is slightly altered, as can be seen in Fig. 13a. The first two-bounce windows in this figure is labeled $m = 7$. This corresponds to the number of oscillations between bounces shown in Fig. 13a. This is smaller than the value $m = 11$ obtained for $H = 0$ (our m corresponds to $n - 1$ in the Ref. [12]). Growing more the parameter H , we see that m decreases - compare Fig. 13b ($H = 0.2H_m$, $m = 4$) with Fig. 13c ($H = 0.4H_m$, $m = 2$). A quantitative view of this decay of m with H is presented in the Fig. 14. There one can see

that m decreases until the value $m = 1$ of the first window for $H = 0.5H_m$. This shows that the analog magnetic field contributes to reduce the order of the first two-bounce windows, approaching to those expected from CSW mechanism. However, this occurs at the price of an increasing distortion around the bounces of $\phi(0, t)$, as can be seen in Figs. 13b and 13c. For $H > H_c \simeq 0.6H_m$ two-bounce windows disappear and the vibrational mode of the boundary now contributes to the production of kink during the scattering.

We have also checked that even in the regime of H connected with an irregular pattern of oscillations between bounces (see for instance Fig. 13c for $H = 0.4H_m$), the classification of m used here is in accord to the CSW mechanism. This was confirmed by the expected linear behavior between the time interval between bounces and the parameter m for both regimes $H = 0.1H_m$ (where the fluctuations are regular) and $H = 0.4H_m$ (where the fluctuations are irregular).

VI. KINK-BOUNDARY

Here we will consider scattering with a kink in the sector $(0, 1)$ with the boundary. The kink is the static solution $\Phi_{1+}(x)$ given by the Eq. (14), now boosted with a velocity v_i with $x(t = 0) = a$ and given by:

$$\Phi_{1+}(v_i, x, t) = \sqrt{\frac{1 + \tanh(\gamma(x - v_i t - a))}{2}}. \quad (41)$$

The Fig. 5 shows that this kink can be connected only with solutions $\tilde{\phi}_1(x)$ and $\tilde{\phi}_3(x)$. In the following we consider separately the two possibilities.

A. Kink- $\tilde{\phi}_1$ boundary

For this solution we consider $-H_m < H < 0$. The initial conditions are

$$\phi(x, 0) = \Phi_{1+}(v, x, 0) + \tilde{\phi}_1(x) - 1, \quad (42)$$

$$\dot{\phi}(x, 0) = \dot{\Phi}_{1+}(v, x, t)|_{t=0}. \quad (43)$$

with $a = -12.50$.

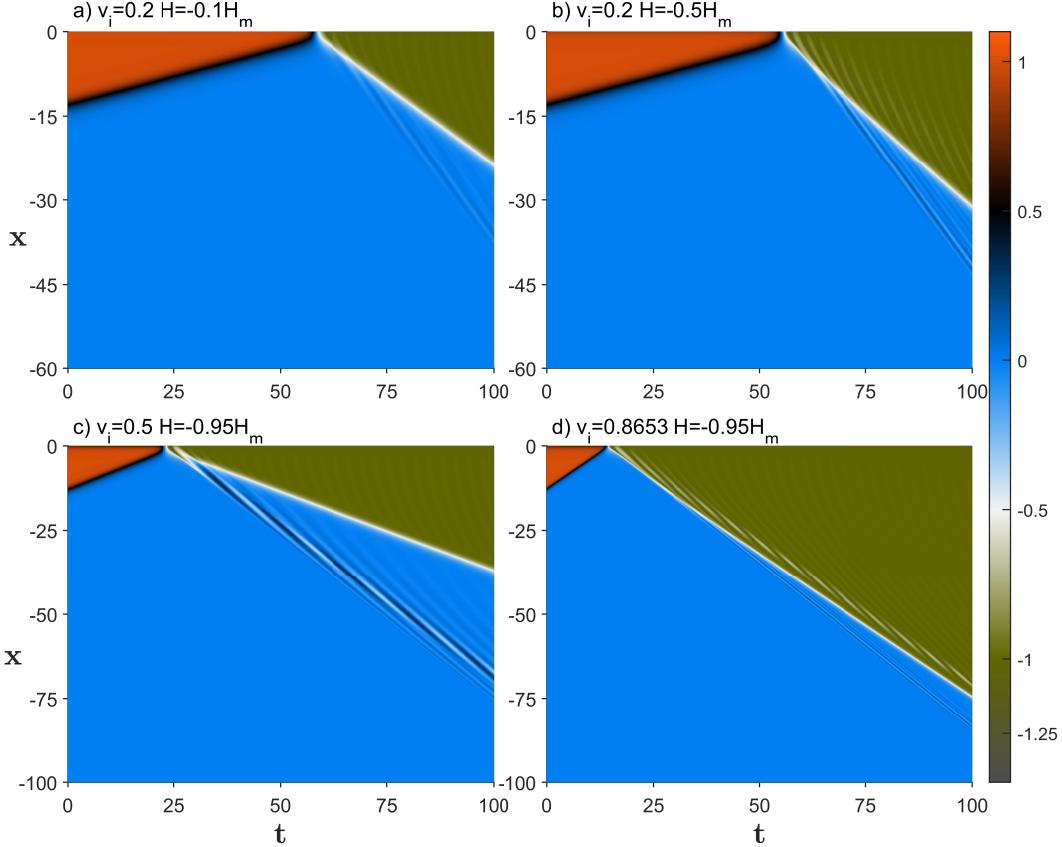


FIG. 15: Φ_{1+} kink scattering with $\tilde{\phi}_1$ boundary for different values of v_i and H , showing: in a) and b), the changing of the topological sector with a produced Φ_{1-} antikink; in c) and d), a produced oscillon and Φ_{1-} antikink.

The Fig. 15 shows different aspects of the scattering process. We found that, as a result of the scattering there is a changing of the topological sector with the production a Φ_{1-} antikink. Note also that the nature of the boundary $\tilde{\phi}_1$ has changed due to the scattering to another boundary $-\tilde{\phi}_3$. In this way we have the process $\Phi_{1+} + \tilde{\phi}_1 \rightarrow \Phi_{1-} + (-\tilde{\phi}_3)$. The final $-\tilde{\phi}_3$ boundary has no bound state, only a continuum of states. The modulus v_f of the velocity of the produced antikink has an intricate dependence with v_i and H , as shown for instance in the Fig. 16. Another interesting effect is the appearing of a travelling oscillon, as shown in the Fig. 15b. This effect starts to appear for $|H| \approx 0.70H_m$ but it is more evident for $|H| > 0.90H_m$. The oscillon has the scalar field around the vacuum $\phi = 0$ when its velocity is larger than v_f , as in the example of the Fig.15c. If its velocity is lower than v_f , the scalar field oscillating around the vacuum $\phi = -1$. Note also that, contrarily to the rich pattern observed for antikink-boundary scattering in the Fig. 10, here we have that for

all phase space (v_i, H) the final state of the boundary is close to the vacuum $\phi = -1$.

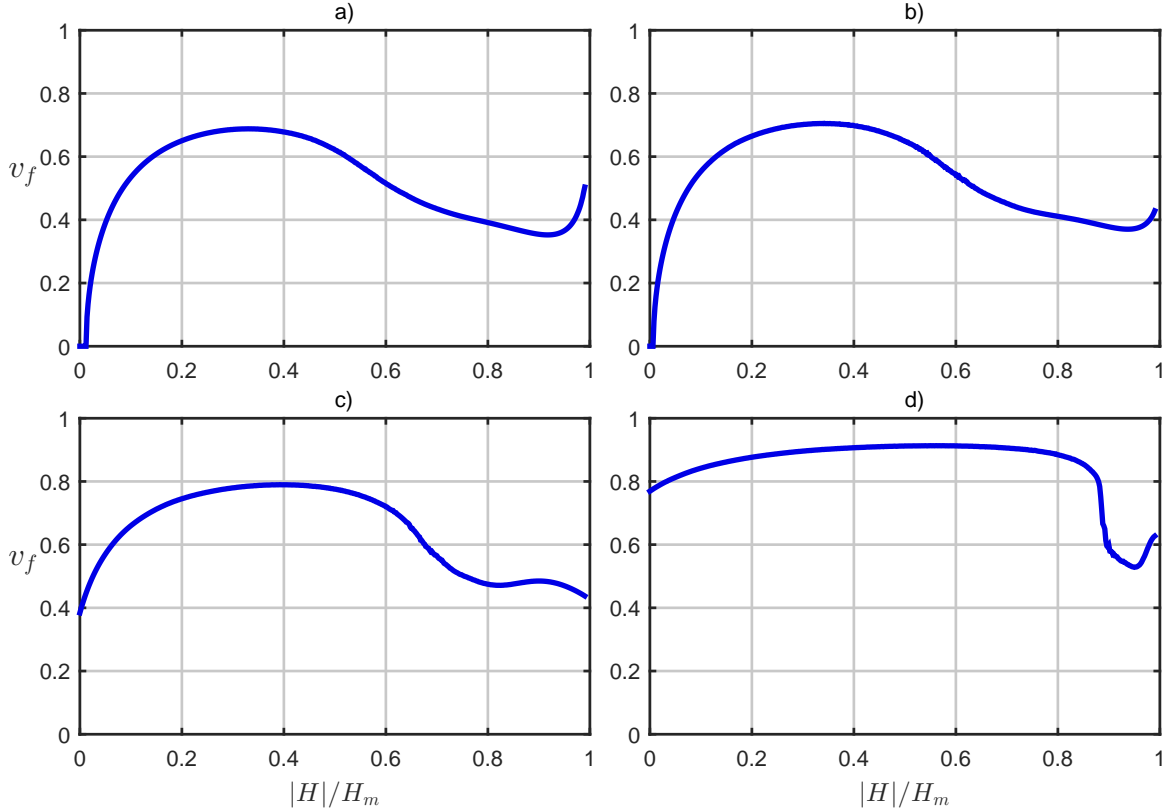


FIG. 16: Final velocity modulus v_f of the produced Φ_{1-} antikink as a function of $|H|/H_m$ with a) $v_i = 0.05$ b) $v_i = 0.20$ c) $v_i = 0.50$ d) $v_i = 0.80$.

B. Kink- $\tilde{\phi}_3$ boundary

For this solution we have $0 \leq H < \infty$. However, to ease the comparison with the other cases, in our simulations we will consider the specific range $0 \leq H \leq H_m$. The initial conditions are

$$\phi(x, 0) = \Phi_{1+}(v, x, 0) + \tilde{\phi}_3(x) - 1, \quad (44)$$

$$\dot{\phi}(x, 0) = \dot{\Phi}_{1+}(v, x, t)|_{t=0}. \quad (45)$$

with $a = -12.50$.

In this case the boundary presents an initially-repulsive force. The Fig. 17 shows the pattern of scattering for different values of v_i and H . The Fig. 18 shows the value of the

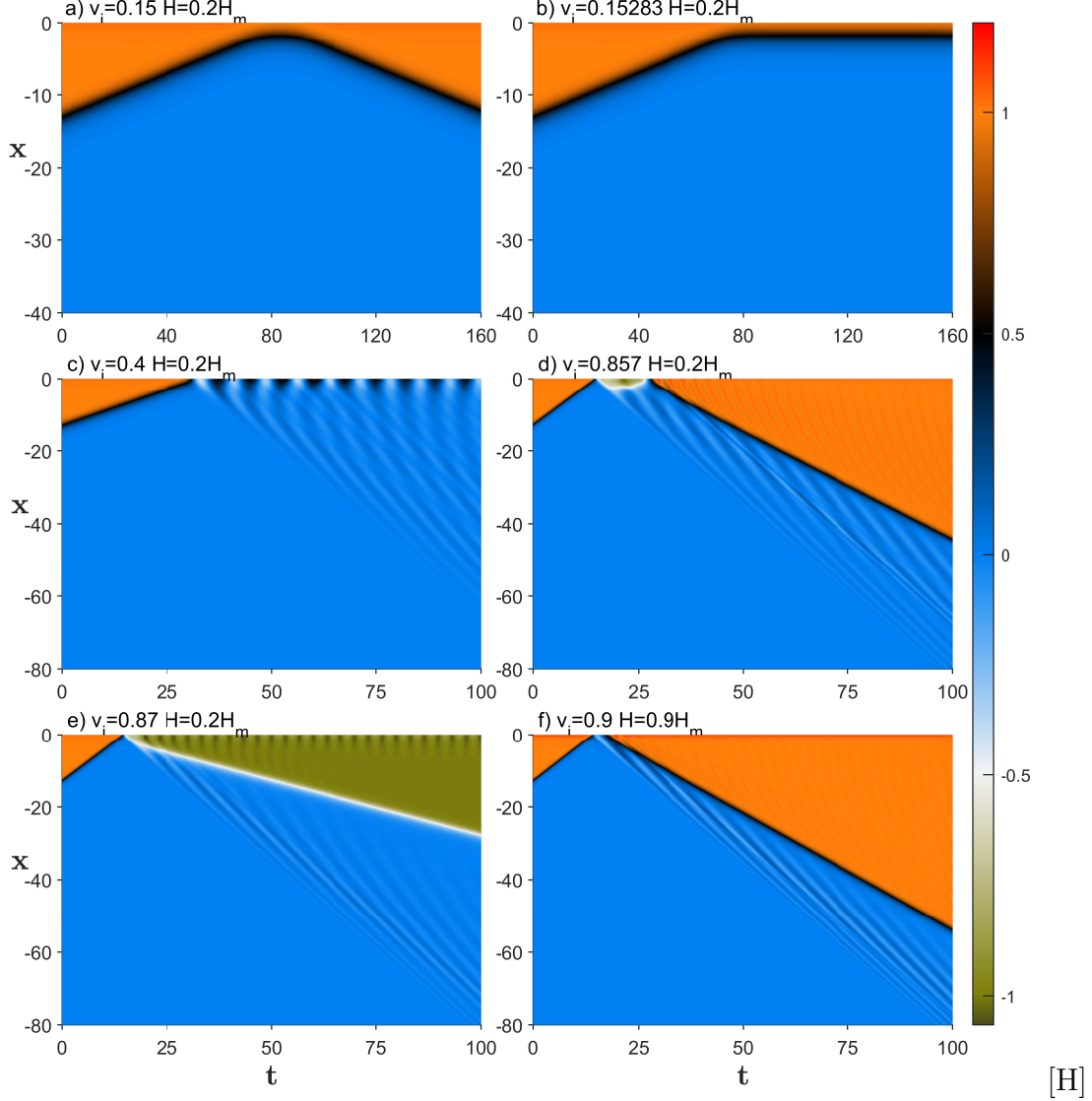


FIG. 17: Φ_{1+} kink scattering with $\tilde{\phi}_3$ boundary, showing a) quasi-elastic return b) kink with energy to reach the energy equilibrium point c) emission of radiation by the unstable ϕ_2 boundary d) Typical collision on top orange region of Fig. 18 e) Inelastic scattering f) Final state for large H .

scalar field at the boundary for a large scale of time. For small initial velocities, the kink do not even reach the boundary at $x = 0$, and the scattering is almost elastic, with a small emission of radiation (see the Fig. 17a). Increasing the value of v_i until a certain velocity v_* , the kink becomes stuck to the boundary, with very low rate of emitted radiation, as shown in the Fig. 17b. This final state is the unstable configuration ϕ_2 . This is supported by energy considerations. Indeed, since there is a small amount of emitted radiation, we can obtain v_* considering the conservation of energy between initial and final states. For the

initial state we have $E_i = \frac{1}{4}\gamma(v_*) + E[\tilde{\phi}_3]$ whereas for the final state we have $E_f = E[\phi_2]$. The equality $E_i = E_f$ gives (see a similar reasoning for the ϕ^4 model in the Ref. [44])

$$v_*(H) = \sqrt{1 - \left[3\phi_2(0)^4 + 3\tilde{\phi}_3(0)^4 - 2\phi_2(0)^2 - 2\tilde{\phi}_3(0)^2 - 1\right]^{-2}}. \quad (46)$$

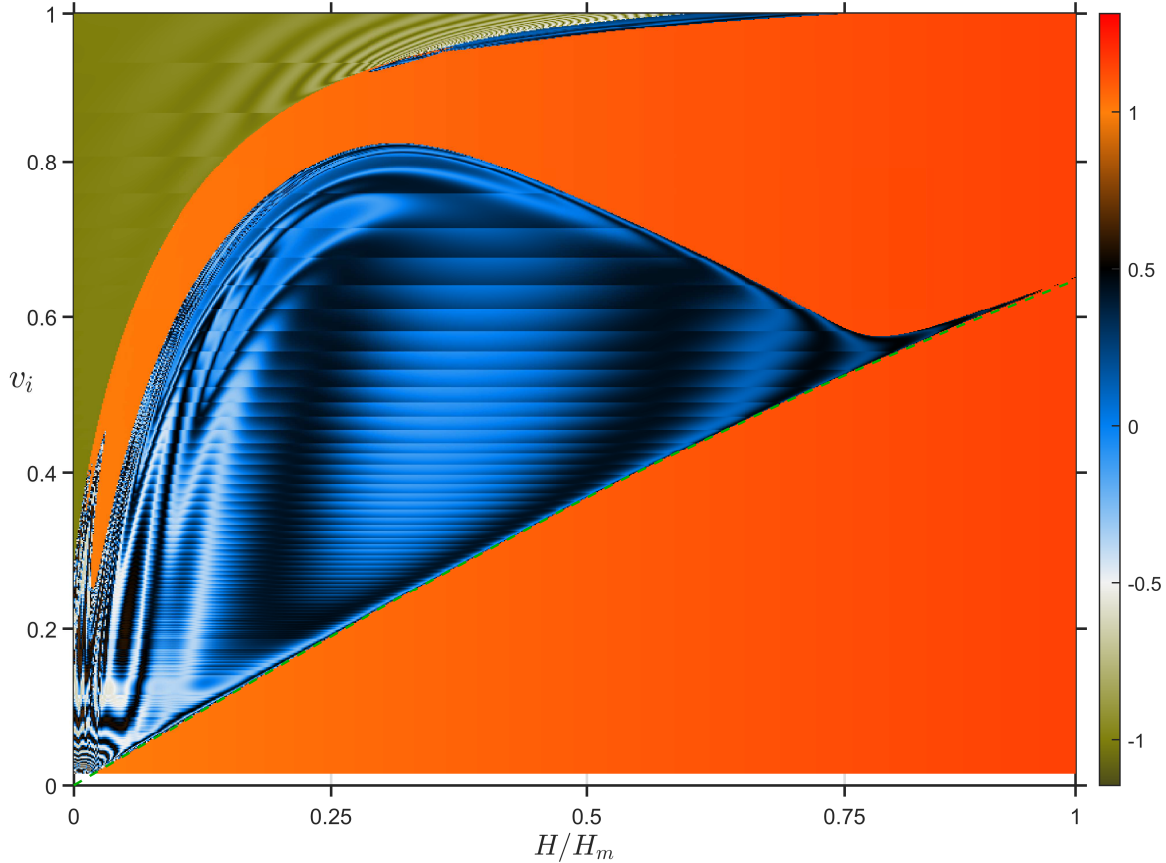


FIG. 18: Final state of the scalar field $\phi(0, t_f)$, with t_f being the nearest integer of $\frac{|a|}{v_i} + 100$.

The curve $v_*(H)$ is included in the Fig. (18) (green traced line). Note the agreement between this figure, which is constructed with the results of numerical solutions of the kink-boundary scattering and the expression given by the Eq. (46). Increasing the initial velocity above v_* , there is an intermediate region where we observe that the kink approaches, overcome the potential barrier and is absorbed by the boundary, that now radiates in a typical pattern of the unstable solution ϕ_2 (see the Fig. 17c and the discussion of the end of Sect. IV). Here one has a process like $\Phi_{1+} + \tilde{\phi}_3 \rightarrow \phi_2$. This type of scattering corresponds to the central blue region of the Fig. 18. Keeping H fixed and increasing v_i , there occurs a

scenario like that of the Fig. 17d where the nature of the $\tilde{\phi}_3$ boundary does not change due to the scattering. There is the emission of a Φ_{1+} kink, followed by the emission of radiation from the continuum states of the boundary. This type of scattering corresponds to the upper orange region of the Fig. 18. Increasing further the velocity, one has the scenario of the Fig. 17e, which shows the changing of the topological sector and the production of an Φ_{1-} antikink. This corresponds to the green region of the Fig.18. The possibility of changing the topological sector decreases for large values of H . Larger values of H in the same orange region of Fig. 18 we have the effect that during the collision the scalar field at the center of mass oscillates around $\phi = 0$, as in the Fig. 17f.

VII. CONCLUSIONS

In this work we have considered the ϕ^6 model with a Neumann boundary condition characterized by the parameter H . We found several solutions for kink, antikink and boundary. Stability analysis for the antikink and kink lead to a translational mode. A similar procedure for the boundary solutions gives the behavior of the squared frequency of discrete modes as a function of H . This resulted in three regular and stable solutions for the boundaries. The study of the unstable boundary was important since the nature of a boundary can be changed to an unstable one due to the scattering process. The changing of the nature of a regular and stable boundary due to the scattering was verified in some examples in two ways: i) a topological argument - the changing of the topological sector, and ii) energy conservation leading to an accurate description of the critical velocity as a function of H . After a period of time without any sensible alteration, and depending on the parameter H , there are two possibilities for the time evolution of an isolated unstable boundary: i) radiation being emitted continuously, or ii) creation of a kink and decaying to a stable boundary. As initial conditions, we considered kink/antikink scattering with regular and stable boundaries.

Our numerical analysis showed that the antikink-boundary scattering model has a rich pattern. We report the following phenomena, depending on the initial velocity and the parameter H : i) the production of a new kink from the boundary at $x = 0$ that travels with the reflected antikink. Such reflected antikink-kink pair can have a finite number of mutual collisions separating afterwards. Other possibility is the pair travelling together and colliding an infinite number of times, in a bion-like state. Such effect was observed previously

in the ϕ^4 model (see the Ref. [44]). ii) the presence of a critical escape velocity, above which the antikink always recedes to $-\infty$ without the production of a new travelling kink at the boundary. iii) the formation of two-bounce windows.

For the kink-boundary scattering here are two possibilities for a regular and stable boundary. For one boundary the scalar field always changes to the other topological sector. As a result, the new boundary emits an antikink with or without an oscillon. Another possibility for the initial boundary has a richer pattern. In this case the interaction with the kink is repulsive. This means that there is a critical velocity where the kink become trapped by the boundary. Depending on the parameters (v_i, H) one can also see the changing of the boundary with the emission of radiation or the changing of the topological sector.

When compared with the results for the ϕ^4 model [44], despite its higher nonlinearity, the structure revealed by the antikink-boundary collisions for the ϕ^6 model is simpler. Indeed, as we saw in Fig. 11, v_c grows monotonically with H for $0 < H < H_m$, favoring the emission of a kink from the boundary. On the contrary, for the ϕ^4 model and $0 < H \lesssim 0.5H_m$, v_c initially decreases with H , favoring the 1-bounce region. Fig. 10 shows that the region close to $H \sim H_m$ for the ϕ^6 model has a clear separation between two regions: 1-bounce (blue) and kink formation from the boundary (red). The corresponding region for the ϕ^4 model (see the Fig. 3 from Ref. [44]) is intricate, and the v_c has no functional form. The complexity of the ϕ^6 model comes from the existence of two topological sectors. Even in one topological sector there are more solutions for kink, antikink and boundaries. This results, for the ϕ^6 model, in different structures for antikink-boundary and kink-boundary scattering and in the possibility of changing the topological sector.

Despite our investigation being mostly numerical, we connected some of the reported effects to the presence of bound states and continuum states in the system antikink-boundary or kink-boundary. Also, our results extended, for $H \neq 0$, the known results for scattering in the full-line.

VIII. ACKNOWLEDGEMENTS

F.C.L, F.C.S., K.Z.N and A.R.G thank FAPEMA - Fundação de Amparo à Pesquisa e ao Desenvolvimento do Maranhão through grants PRONEX 01452/14, PRONEM 01852/14, Universal 01061/17, 01191/16, 01332/17, 01441/18 and *BD* – 00128/17. A.R.G thanks

CNPq (brazilian agency) through grants 437923/2018-5 and 311501/2018-4 for financial support. This study was financed in part by the Coordenação de Aperfeiçoamento de Pessoal de Nível Superior - Brasil (CAPES) - Finance Code 001. Gomes thanks R. Casana for discussions. The authors thank T. Romańczukiewicz, P. Dorey and Ya. Shnir for the interesting comments about scattering with other boundaries and the existence of internal modes of the boundary solution.

- [1] T. Dauxois, M. Peyrard, *Physics of Solitons*, Cambridge University Press, Cambridge (2006).
- [2] E. J. Weinberg, *Classical Solutions in Quantum Field Theory*, Cambridge Monographs on Mathematical Physics (Cambridge University Press, Cambridge, England, 2012).
- [3] W. B. Cardoso, J. Zeng, A. T. Avelar, D. Bazeia and B. A. Malomed, Bright solitons from the nonpolynomial Schrödinger equation with inhomogeneous defocusing nonlinearities, *Phys. Rev. E* 88, 025201 (2013).
- [4] T. Vachaspati, *Kinks and Domain Walls*, Cambridge Univ. Press, Cambridge, 2006.
- [5] T. Sugiyama, *Kink-Antikink Collisions in the Two-Dimensional ϕ^4 Model*, *Prog. Theor. Phys.* 61, 1550 (1979).
- [6] M. Moshir, *Soliton-antisoliton scattering and capture in $\lambda\phi^4$ theory*, *Nucl. Phys. B* 185, 318 (1981).
- [7] C. A. Wingate, Numerical Search for a ϕ^4 Breather Mode, *SIAM J. Appl. Math.* 43(1), 120-140 (1983).
- [8] D. K. Campbell, J. S. Schonfeld, C. A. Wingate, Resonance Structure in Kink-antikink interactions in ϕ^4 theory, *Physica. D* 9, 1 (1983).
- [9] T. I. Belova, A. E. Kudryavtsev, *Quasi-periodic orbits in the scalar classical $\lambda\phi^4$ field theory*, *Physica D* 32, 18 (1988).
- [10] P. Anninos, S. Oliveira, R. A. Matzner, Fractal structure in the scalar $\lambda\phi^4$ theory, *Phys. Rev. D* 44, 1147 (1991).
- [11] R. H. Goodman, R. Haberman, Kink-Antikink Collisions in the ϕ^4 Equation: The n-Bounce Resonance and the Separatrix Map, *SIAM J. Appl. Dyn. Syst.* 4, 1195 (2005).
- [12] P. Dorey, K. Mersh, T. Romanczukiewicz, Y. Shnir, Kink-Antikink Collisions in the ϕ^6 Model, *Phys. Rev. Lett.* 107, 091602 (2011).

- [13] Vakhid A. Gani, Alexander E. Kudryavtsev, Mariya A. Lizunova, Kink interactions in the $(1 + 1)$ -dimensional ϕ^6 model, Phys. Rev. D 89, 125009 (2014).
- [14] Vakhid A. Gani, Vadim Lensky, Mariya A. Lizunova, Kink excitation spectra in the $(1+1)$ -dimensional ϕ^8 model, JHEP 08 (2015) 147.
- [15] P. Dorey, T. Romanczukiewicz, Resonant kink-antikink scattering through quasinormal modes, Phys. Lett. B, 779, 117 (2018).
- [16] Oscillons in the presence of external potential, T. Romanczukiewicz, Y. Shnir, JHEP 1, 101 (2018).
- [17] D. K. Campbell, M. Peyrard, P. Soldano, *Kink-antikink interactions in the double sine-gordon equation*, Physica D 19, 165 (1986).
- [18] M. Peyrard, D. K. Campbell, Kink-antikink interactions in a modified sine-Gordon model, Physica D Nonlinear Phenomena 9 (1983) 3351.
- [19] D. K. Campbell, M. Peyrard, *Solitary wave collisions revisited*, Phys. D, 18 (1986), pp. 4753.
- [20] V. A. Gani, A. E. Kudryavtsev, *Kink-antikink interactions in the double sine-Gordon equation and the problem of resonance frequencies*, Phys. Rev. E 60, 3305-3309 (1999).
- [21] D. Bazeia, E. Belendryasova, V. A. Gani, Scattering of kinks of the sinh-deformed ϕ^4 model, Eur. Phys. Journ. C 78, 340 (2018).
- [22] F.C. Simas, Adalto R. Gomes, K.Z. Nobrega, J.C.R.E. Oliveira, Suppression of two-bounce windows in kink-antikink collisions, JHEP 1609 (2016) 104.
- [23] F.C. Simas, A.R. Gomes, K.Z. Nobrega, Degenerate vacua to vacuumless model and kink-antikink collisions, Phys. Lett. B 775 (2017) 290.
- [24] T. S. Mendonça, H.P. de Oliveira, A note about a new class of two-kinks JHEP 1506 (2015) 133.
- [25] T. S. Mendonça, H.P. de Oliveira, The collision of two-kinks defects, JHEP 1509 (2015) 120.
- [26] V. A. Gani, A. M. Marjaneh, A. Askari, E. Belendryasova, D. Saadatmand, Scattering of the double sine-Gordon kinks, Eur. Phys. Journ. C 78, 345 (2018).
- [27] Aliakbar Moradi Marjaneh, Vakhid A. Gani, Danial Saadatmand, Sergey V. Dmitriev, A. Kurosh Javidan, Multi-kink collisions in the ϕ^6 model, JHEP 1707 (2017) 028.
- [28] A. Halavanau, T. Romanczukiewicz, Ya. Shnir, Resonance structures in coupled two-component ϕ^4 model, Phys. Rev. D86 (2012) 085027.
- [29] A. Alonso-Izquierdo, Reflection, transmutation, annihilation and resonance in two-component

- kink collisions, Phys.Rev. D97 (2018) no.4, 045016.
- [30] A. Alonso-Izquierdo, Kink dynamics in a system of two coupled scalar fields in two space-time dimensions, Physica 365 (2018) 12-26.
- [31] A. Alonso-Izquierdo, Asymmetric kink scattering in a two-component scalar field theory model, Commun. in Nonlinear Science and Num. Sim., 75, 200-219 (2019).
- [32] Mustafa A. Amin, Eugene A. Lim, I-Sheng Yang, A Clash of Kinks: Phase shifts in colliding non-integrable solitons, Phys. Rev. Lett. 111, 224101 (2013).
- [33] E. Sklyanin, Boundary conditions for integrable equations, Funct. Anal. Appl. 21 (1987) 164
- [34] E. Sklyanin, Boundary conditions for integrable quantum systems, J. Phys. A 21 (1988) 2375 [INSPIRE].
- [35] V.O. Tarasov, The integrable initial-boundary value problem on a semiline: nonlinear Schrodinger and sine-Gordon equations, Inverse Probl. 7 (1991) 435.
- [36] I.T. Habibullin, The Bäcklund transformation and integrable initial boundary value problems, Math. Notes 49 (1991) 18.
- [37] I.T. Habibullin, Integrable initial-boundary-value problems, Theor. Math. Phys. 86 (1991) 28.
- [38] I.T. Habibullin, Sine-Gordon equation on the semi-axis, Theor. Math. Phys. 114 (1998) 90.
- [39] S. Ghoshal and A.B. Zamolodchikov, Boundary S-matrix and boundary state in two-dimensional integrable quantum field theory, Int. J. Mod. Phys. A 9 (1994) 3841 [Erratum ibid. A 9 (1994) 4353].
- [40] T. Inami, S. Odake and Y.-Z. Zhang, Supersymmetric extension of the sine-Gordon theory with integrable boundary interactions, Phys. Lett. B 359 (1995) 118.
- [41] R.I. Nepomechie, The boundary supersymmetric sine-Gordon model revisited, Phys. Lett. B 509 (2001) 183.
- [42] A.R. Aguirre, J.F. Gomes, L.H. Ymai and A.H. Zimerman, N=1 super sinh-Gordon model in the half line: Breather solutions, JHEP 04 (2013) 136.
- [43] A.R. Aguirre, J.F. Gomes, N.I. Spano, A.H. Zimerman, Type-II super-Bäcklund transformation and integrable defects for the N=1 super sinh-Gordon model, JHEP06(2015)125.
- [44] P. Dorey, A. Halavanau, J. Mercer, T. Romanczukiewicz, Y. Shnir *Boundary scattering in the ϕ^4 model*, JHEP05(2017)107.
- [45] R. Arthur, P. Dorey and R. Parini, Breaking integrability at the boundary: the sine-Gordon model with Robin boundary conditions, J. Phys. A 49 (2016) 165205.

- [46] John T. Giblin, Lam Hui, Eugene A. Lim, I-Sheng Yang, *How to Run Through Walls: Dynamics of Bubble and Soliton Collisions*, Phys.Rev. D82 (2010) 045019.
- [47] J. Branden, J. R. Bond, L. Mersini-Houghton, *Cosmic bubble and domain wall instabilities I: parametric amplification of linear fluctuations*, JCAP 03 (2015) 007.
- [48] P. Ahlqvist, K. Eckerle, B. Greene, *Kink Collisions in Curved Field Space*, JHEP 1504 (2015) 059.
- [49] T. W. Kibble, Acta Phys. Polon B13, 723 (1982).
- [50] T. Romanczukiewicz, *Could the primordial radiation be responsible for vanishing of topological defects?*, Phys. Lett. B 773 (2017) 295.
- [51] T. Mashoff, M. Pratzner, V. Geringer, T. J. Echtermeyer, M. C. Lemme, M. Liebmann, and M. Morgenstern, Nano Letters 10, 461 (2010).
- [52] R. D. Yamaletdinov, V. A. Slipko, Y. V. Pershin, *Kinks and antikinks of buckled graphene: A testing ground for the ϕ^4 field model*, Phys. Rev. B 96, 094306 (2017).
- [53] R. D. Yamaletdinov, T. Romanczukiewicz, Y. V. Pershin, *Manipulating graphene kinks through positive and negative radiation pressure effects*, Carbon 141, 253-257 (2019).
- [54] P. Forgács, A. Lukács, T. Romańczukiewicz, *Negative radiation pressure exerted on kinks*, Phys. Rev. D 77 (2008) 125012
- [55] A.J. Heeger, S. Kivelson, J.R. Schrieffer, and W.P. Su. *Solitons in conducting polymers*. Reviews of Modern Physics 60, 781 (1988).
- [56] Y. Lu. *Solitons and Polarons in Conducting Polymers*. World Scientific Publisher, Singapore, 1988.
- [57] S. Roth, D. Carroll, *One-Dimensional Metals*, WILEY-VCH, Weinheim, 2004.
- [58] W. P. Su, J. R. Schrieffer, A. J. Heeger, *Solitons in Polyacetylene*, Phys. Rev. Lett. 42, 1698 (1979).
- [59] Kivelson, S. and Heeger, A. J. , *1ST-Order Transition to a Metallic State in Polyacetylene: A Strong-coupling Polaronic Metal*, Phys. Rev. Lett. 55, 308 (1985).
- [60] L. Bernasconi, *Chaotic Soliton Dynamics in Photoexcited trans-Polyacetylene*, J. Phys. Chem. Lett. 6, 5, 908 (2015).
- [61] W. P. Su, J. R. Schrieffer, *Soliton dynamics in polyacetylene*, Proc. Natl. Acad. Sci. USA 77, 5626 (1980).
- [62] S. Kivelson, D. E. Heim, *Hubbard versus Peierls and the Su-Schrieffer-Heeger model of poly-*

- acetylene*, Phys. Rev. D 26, 4278 (1982).
- [63] R. S. Pfeiffer, G. Yoder, and A.-B. Chen, *Ground state and excitations in polyacetylene chains*, Phys. Rev. B 54, 1735 (1996).
- [64] E. B. Bogomolny, *The stability of classical solutions*, Sov. J. Nucl. Phys. 24, 449 (1976).
- [65] M. K. Prasad, C. M. Sommerfield, *Exact Classical Solution for the 't Hooft Monopole and the Julia-Zee Dyon*, Phys. Rev. Lett. 35, 760 (1975).
- [66] M. A. Lohe, Phys. Rev. D 20, 3120 (1979).
- [67] P.M. Morse and H. Feshbach, *Methods of Theoretical Physics*. McGraw-Hill, New York, 1953.